Available online at www.sciencedirect.com
ScienceDirect
Journal of the European Ceramic Society 29 (2009) 1361–1369
www.elsevier.com/locate/jeurceramsoc

High strength porous alumina by spark plasma sintering

Dibyendu Chakravarty [a,*], Hayagreev Ramesh [b], Tata N. Rao [a]

[a] International Advanced Research Centre for Powder Metallurgy and New Materials (ARCI), Balapur P.O., Hyderabad 500005, Andhra Pradesh, India
[b] Department of Metallurgical and Materials Engineering, Indian Institute of Technology Madras, Chennai 600036, Tamil Nadu, India

Received 27 June 2008; received in revised form 13 August 2008; accepted 15 August 2008
Available online 1 October 2008

Abstract

High strength porous alumina was fabricated by spark plasma sintering (SPS) at temperatures between 1000 and 1200 °C with nanocrystalline $Al(OH)_3$ as the starting powder without any seeds, dopants or inclusions. Decomposition of the $Al(OH)_3$ produced a series of transitional alumina phases depending on sintering temperature and pressure and finally the stable α-alumina phase was obtained. A network of continuous pores with unimodal pore size distribution was estimated by mercury porosimetry and BET surface area measurements, with the porosity ranging between 20% and 60% based on sintering conditions. Predominance of fine grains and extensive necking between them led to better strength in the sintered samples. The bending strength of the sintered compacts rapidly increased with sintering temperature while retaining reasonable porosity suitable for practical applications. The results clearly indicate that in situ phase formation of α-Al_2O_3 and θ-Al_2O_3 provides strength and porosity, respectively. Phase transformation, pore morphology and microstructure evolution were also studied.

Keywords: Spark plasma sintering; Grain size; Porosity; Strength; $Al(OH)_3$

1. Introduction

Porous ceramic materials have several applications because of their high separation efficiency, corrosion resistance, high permeability and surface area as well as mechanical strength and structural stability. They are widely used as ceramic membranes, filters, desiccants, catalyst supports and also as bone replacements and structural components.[1,2] Industries based on porous ceramic materials are rapidly developing; manufacturing micro- and nano-particle filters/membranes having pore size of 0.1 μm or less are widely prevalent. Porous alumina having a continuous network of nanopores in the microstructure is well suited for such applications as alumina has high strength, wear and abrasion resistance and the capability to withstand corrosive environment.

Conventionally, porous alumina is fabricated by partial sintering of fine grained alumina powders with or without transitional alumina phases such as boehmite,[3] γ-Al_2O_3,[4] θ-Al_2O_3,[5] and $Al(OH)_3$.[6] Besides, sol–gel processing,[7] and starch consolidation method[8] for fabricating porous ceramic bodies have also been reported. Mechanical properties of porous alumina have been studied extensively over the years. Deng et al.[6] studied the effect of $Al(OH)_3$ on elastic modulus, fracture strength and fracture toughness of pure alumina. Hardy and Green[9] studied the effect of sintering temperature on strength, Young's modulus and fracture toughness of alumina. Ostrowski and Rödel[10] studied the evolution of Young's modulus with porosity for hot pressing and free sintering. Claussen et al.[11] fabricated porous alumina by a reaction bonding method and observed higher strength than that fabricated by partial sintering. Oh et al.[12] have used spark plasma sintering (SPS) technique to make porous ceramics using alumina and alumina-SiC nanocomposites and observed enhanced necking and moderate fracture strength in the materials. Jayaseelan et al.[13] studied the effect of dopants such as MgO and TiO_2 on densification and mechanical behavior of porous alumina using SPS technique. In both these papers[12,13] α-Al_2O_3 has been used as the starting powder, as it is reported to be necessary for good sinterability,[1] and additives were used to improve strength. There are no reports on using $Al(OH)_3$ alone to obtain porous components either by conventional sintering or SPS, in spite of its importance in preparation of

* Corresponding author.
E-mail addresses: dibyenduc@arci.res.in (D. Chakravarty), tatanrao@gmail.com (T.N. Rao).

0955-2219/$ – see front matter © 2008 Elsevier Ltd. All rights reserved.
doi:10.1016/j.jeurceramsoc.2008.08.021

Table 1
Sintering conditions, porosity, average grain size, bending strength and surface area of SPS samples

Sintering temperature (°C)	Applied pressure (MPa)	% porosity	Average grain size (μm)	Bending strength (MPa)	Surface area (m^2/g)
1000	10	63.0 ± 3	–	3^{+1}_{-1}	80 ± 5
1050	10	55.5 ± 3	–	10^{+3}_{-2}	58 ± 5
1050	20	40.0 ± 4	0.05	50^{+6}_{-8}	30 ± 3
1050	30	25.0 ± 4	0.15	250^{+12}_{-10}	8 ± 2
1050	50	20.0 ± 3	0.2	400^{+15}_{-25}	4 ± 1
1100	10	30.5 ± 5	0.1	150^{+10}_{-8}	10 ± 2
1150	10	25.0 ± 3	0.15	250^{+9}_{-14}	7 ± 1
1200	10	20.0 ± 5	0.2	375^{+20}_{-15}	4 ± 1

porous components due to its large volume contraction during sintering.

In the present work we demonstrate, for the first time, the fabrication of porous alumina by SPS using nanocrystalline $Al(OH)_3$ exclusively as the starting material without any additives or dopants. SPS of nanocrystalline $Al(OH)_3$ has been attempted to study the effect of sintering parameters on strength and porosity. The focus was also on studying the changes in pore morphology and pore size distribution along with gradual phase and microstructure evolution with temperature and pressure under SPS conditions.

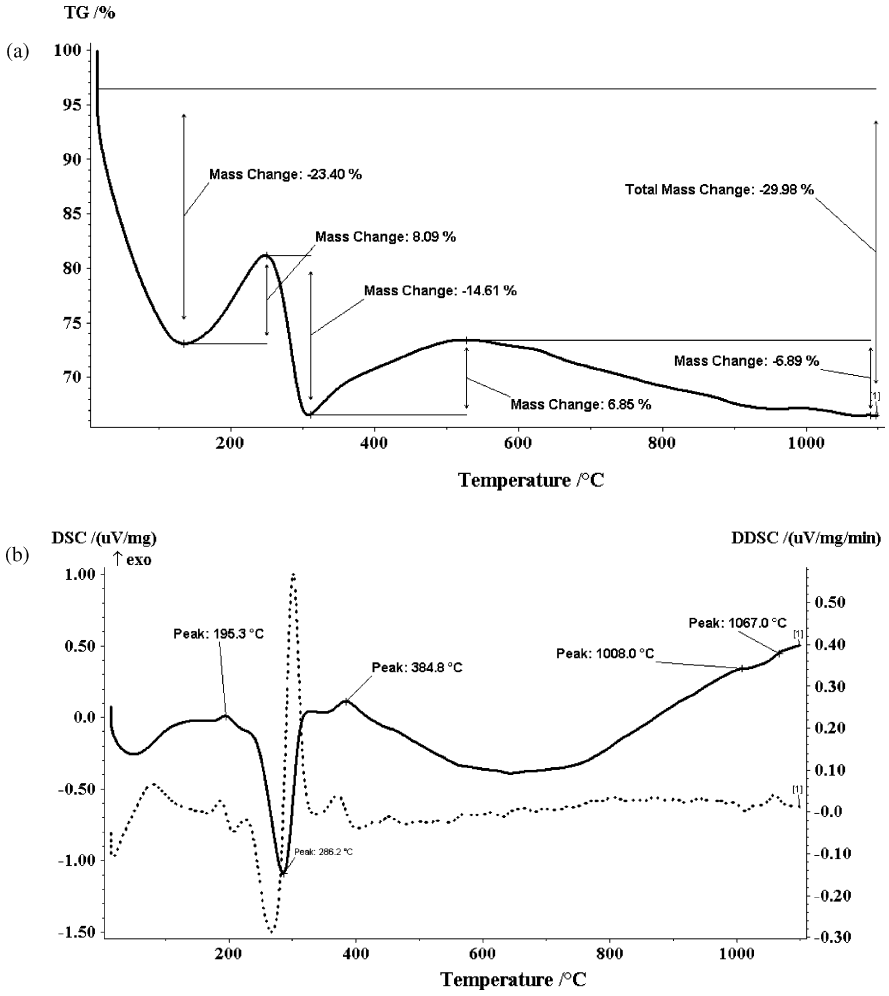

Fig. 1. (a) Thermogravimetric analysis of starting $Al(OH)_3$ powder. (b) Differential scanning calorimetry of starting $Al(OH)_3$ powder.

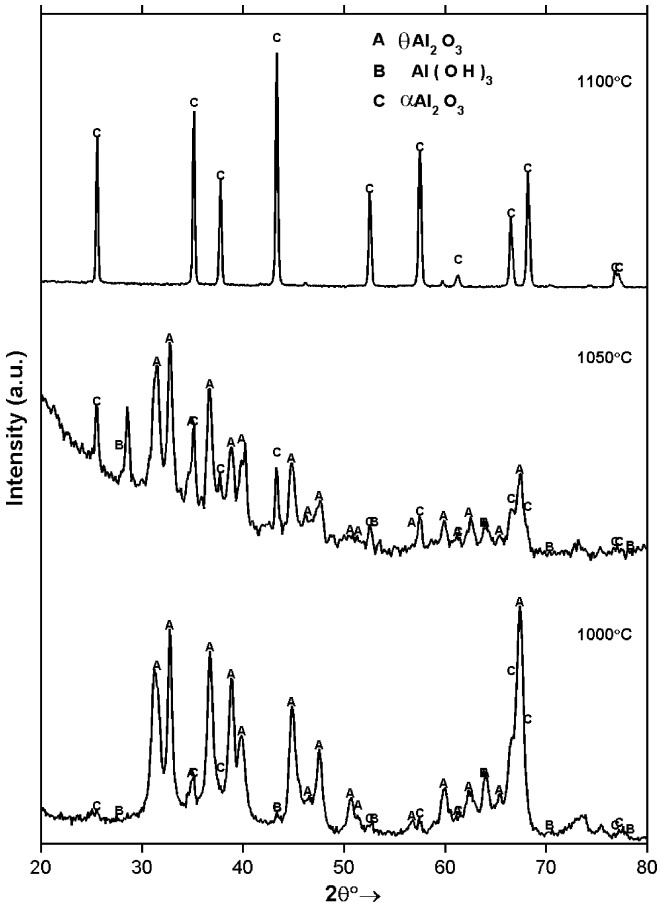

Fig. 2. Phase transformation with temperature at constant pressure of 10 MPa.

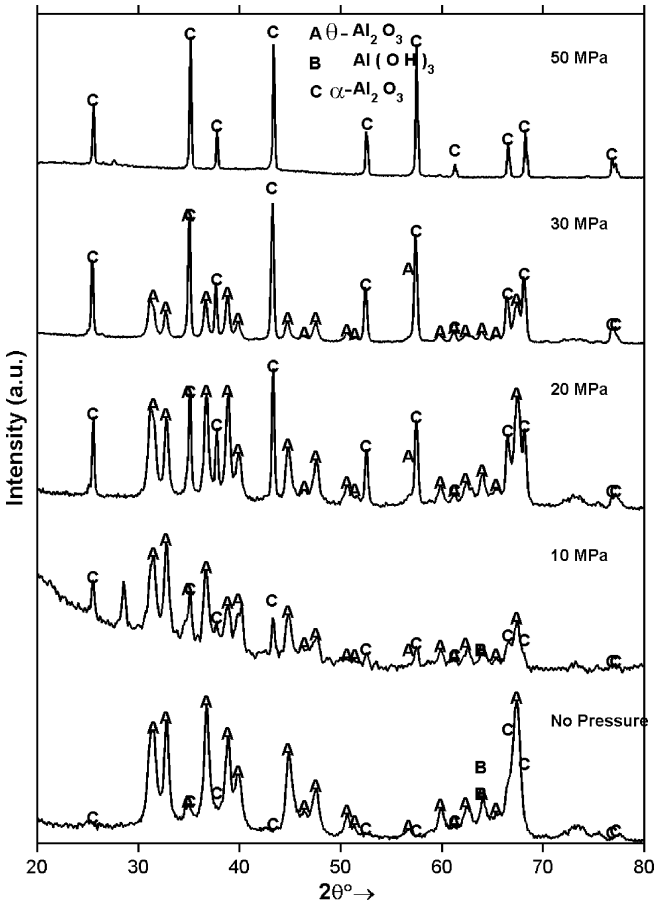

Fig. 3. Phase transformation with pressure at constant temperature of 1050 °C.

2. Experimental procedure

The starting powder was prepared by hydrolysis of aluminum nanopowders produced by the Vapour Condensation by Levitating Drop Inflow (VCLDI) method.[14] Aluminum powder was added to boiling water and stirred which led to a change in color of the powder from grey to milky white along with a hissing sound due to evolution of hydrogen gas. The slurry was allowed to cool overnight; a sediment settled down and the water collected at the top was decanted. The wet sediment was dried at 120 °C to obtain a white powder.

2.1. Spark plasma sintering

Spark plasma sintering of the $Al(OH)_3$ powder was carried out under a vacuum of 6 Pa in a Dr. Sinter 1050 apparatus (Sumitomo Coal Mining Co. Ltd., Japan) with pulse duration of 3.3 ms, and a pulse on/off ratio of 12/2. A graphite die was used for the runs. Sintering was carried out between 1000 and 1200 °C at intervals of 50 °C. A uniaxial pressure of 10 MPa was applied during sintering at all temperatures. Based on the XRD and mercury porosimetry results of these compacts, a further set of samples were sintered at 1050 °C by varying the pressures, to evaluate the effect of pressure on phase change and pore size distribution. The heating rate was constant at 175 °C/min for all the runs and the soaking time was kept constant at 2 min. Temperature measurement and control was through a radiation pyrometer. Shrinkage, displacement, heating current and voltage were also recorded during sintering.

2.2. Characterization

The final densities of the sintered compacts were determined by dimensional measurements and then by the Archimedes' method with deionized water as the immersion medium following ASTM C 373-88 standard.[15]

The decomposition reaction of $Al(OH)_3$ was analyzed by thermogravimetry (TG) and differential scanning calorimetry (DSC) analysis (NETZSCH, STA 409 PC, Germany) from room temperature to 1100 °C in air, with a ramping rate of 10 °C/min.

X-ray diffractometer (Bruker AXS, Germany) was used to analyze the phases and crystal size of the starting powder using Scherrer formula and also the phases of the specimens sintered at different temperatures and pressures.

The pore size distribution of the sintered porous alumina specimens was measured by mercury intrusion porosimetry (POREMASTER, Quantachrome Instruments, FL 33426). To guarantee the reliability of the results, pore size distribution for one of the samples was also measured using the Brunauer–Emmett–Teller (BET) method, by means of N_2 adsorption at −196.15 °C (Model ASAP 2020, Micromeritics, AT).

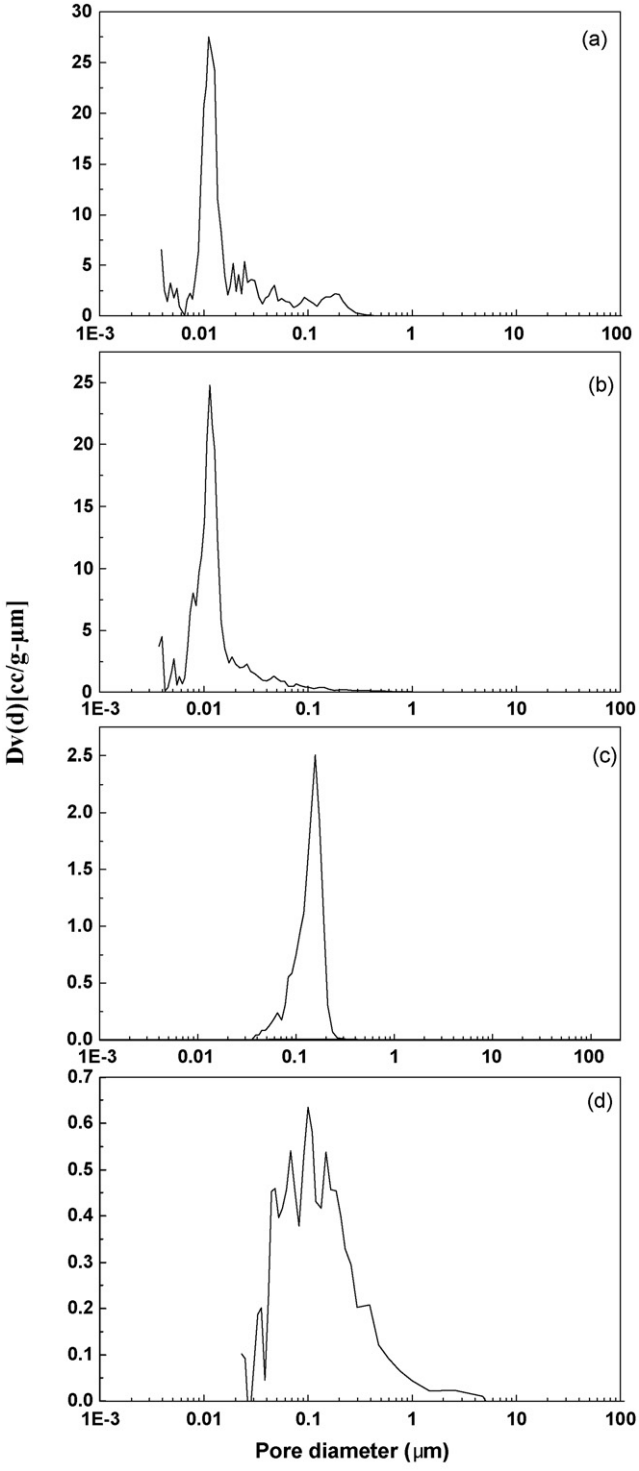

Fig. 4. Pore size distribution at (a) 1000 °C, (b) 1050 °C, (c) 1100 °C and (d) 1150 °C at constant pressure of 10 MPa.

The sintered specimens being highly fragile and porous, it was difficult to prepare samples for microstructure analysis. Instead, the morphology and pore structure of the porous alumina were observed using freshly fractured surface of the sintered specimens by scanning electron microscopy (Model S-4300SE/N, Hitachi, Japan).

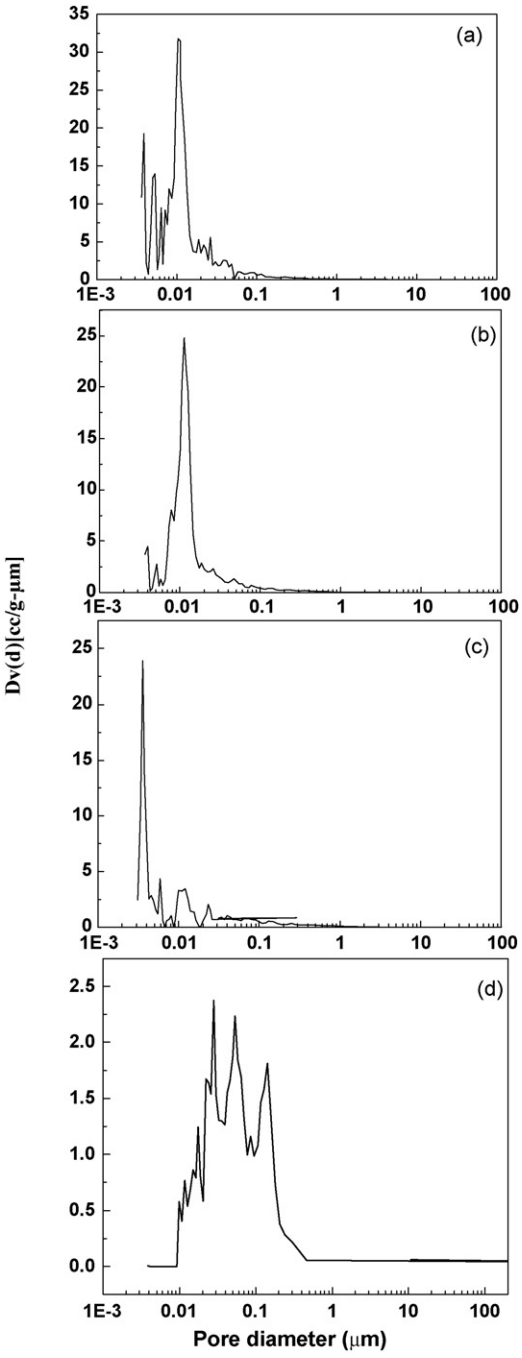

Fig. 5. Pore size distribution at (a) 10 MPa, (b) 20 MPa, (c) 30 MPa and (d) 50 MPa at constant temperature of 1050 °C.

The biaxial bending test (ball-on-ring) was performed in a Universal Testing Machine (UTM Model No.: 5500R, INSTRON, Grove City, PA 16127) with a crosshead speed of 0.5 mm/min and the strength was calculated using the following equation as per ASTM standard 394-78[16]:

$$\sigma_f = \frac{3W(1+\nu)[1+2\ln(D_s/b)+\{1-(b^2/2D_s^2)\}(D_s/D)^2(1-\nu)/(1+\nu)]}{4\pi B^2} \quad (1)$$

where W is the fracture load in N, D_s the diameter of the support circle (16 mm), b the diameter of the area with uniform

load ($b = 0.66B$), B the thickness in mm and D is the diameter of the sample (20 mm). The as-sintered cylindrical samples were polished with diamond paste up to 1 μm grit and then with colloidal alumina with grain size 0.05 μm to make both the faces flat and parallel to each other, as required for ball-on-ring tests. No other specimen preparations are required for this method. Strength values reported was the average of five samples for each sintering condition and variation of the readings between maximum and minimum values are indicated in Table 1.

3. Results and discussion

3.1. Powder characteristics

The powder obtained by hydrolysis of the aluminum nanopowders was checked for phase analysis and grain size by X-ray diffraction. Peaks of $Al(OH)_3$ alone were obtained, proving thereby that the transformation of aluminum into $Al(OH)_3$ was complete. The particle size of the starting powder obtained using Scherrer formula was around 20 nm.

The TG and DSC curves of the starting $Al(OH)_3$ powder are shown in Fig. 1. The TG plot, Fig. 1a, reveals an initial weight loss due to evolution of OH^- ions followed by a heat-absorption peak at 286 °C, Fig. 1b, probably corresponding to bayerite to boehmite phase transformation. The subsequent mass changes as shown in Fig. 1a are due to formation of the transition alumina phases. There is a hump at ∼1067 °C as shown in Fig. 1b which probably corresponds to θ → α-alumina transformation, a fact that is corroborated from XRD plots shown subsequently.

3.2. Phase transformation

Phase transformation of the starting powder with temperature was analyzed by X-ray diffraction as shown in Fig. 2. It was observed that the $Al(OH)_3$ powder almost got fully converted to θ-alumina by 1000 °C, with only trace amount of the powder left unconverted. At 1050 °C there was a mixture of θ- and α-alumina phases. At 1100 °C and above only the stable α-alumina phase was observed.

With gradual increase in pressure at 1050 °C, the amount of α-alumina phase increased with simultaneous decrease in θ-alumina phase, as shown in Fig. 3. Though the θ → α-alumina transition took place at ∼1067 °C in absence of any applied pressure, with pressure the transition temperature decreased gradually. This could probably be due to an enhancement of the oxygen-atom diffusion mechanism for θ → α-alumina transition, as reported by Kao and Wei,[17] under spark plasma sintering conditions. Hence, an increased percentage of α-alumina was observed with increasing pressure from 10 to 50 MPa at 1050 °C.

3.3. Pore morphology and distribution

The pore size distributions at different sintering temperatures and pressures are shown in Figs. 4 and 5, respectively.

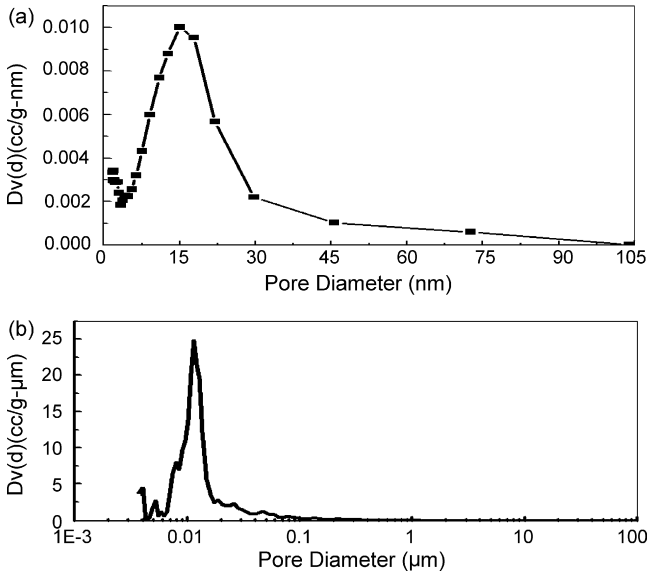

Fig. 6. (a) Pore size distribution from BET analysis. (b) Pore size distribution from mercury porosimetry.

The pores have unimodal distribution, unlike a bimodal distribution as reported by Deng et al.[1] It was observed that with increased temperature and pressure the distribution peaks gradually shifted towards larger size. At 1000 and 1050 °C the pore size distribution were extremely narrow and varied between 3 and 50 nm at 10 MPa pressure. Beyond 1100 °C the distribution became wider. This indicates that the pores were stable and grew during sintering which is contrary to the normally observed phenomena that pores shrink and pore size distribution moves towards smaller size with increasing sintering temperature. This was probably due to the volume contraction during decomposition of $Al(OH)_3$ which leaves vacant spaces around the decomposing particles leading to broader pore channels with increased sintering temperature, as explained elaborately by Deng et al.[1] A comparison of the pore size distribution by mercury porosimetry and BET is shown in Fig. 6. It shows a marked similarity in terms of the nature of the curves and the pore size distribution values confirming the reported results to be reliable.

Increase in pore size distribution was also observed with increasing pressure at a constant temperature of 1050 °C. With pressures up to 30 MPa the pore size distribution range was 3–50 nm whereas with pressures greater than 30 MPa, the range became broader and at 50 MPa it was 0.1–1 μm. This was probably due to volume reduction accompanied by the θ to α phase transformation[17] with gradual increase in pressure. Falamaki et al.[2] had observed similar trends in pore size distribution in porous alumina samples and attributed such a trend to increase in permeability and decrease in tortuosity.

From conditions of pore stability,[18] it is known that there exist a critical coordination number of grains surrounding a pore during sintering. If the actual number of grains surrounding the pore is more than the critical coordination number, the pore is stable and grows, in reverse situations the pore contracts. The increase in pore size with increased temperatures was due to the large coordination number of grains around the pores.

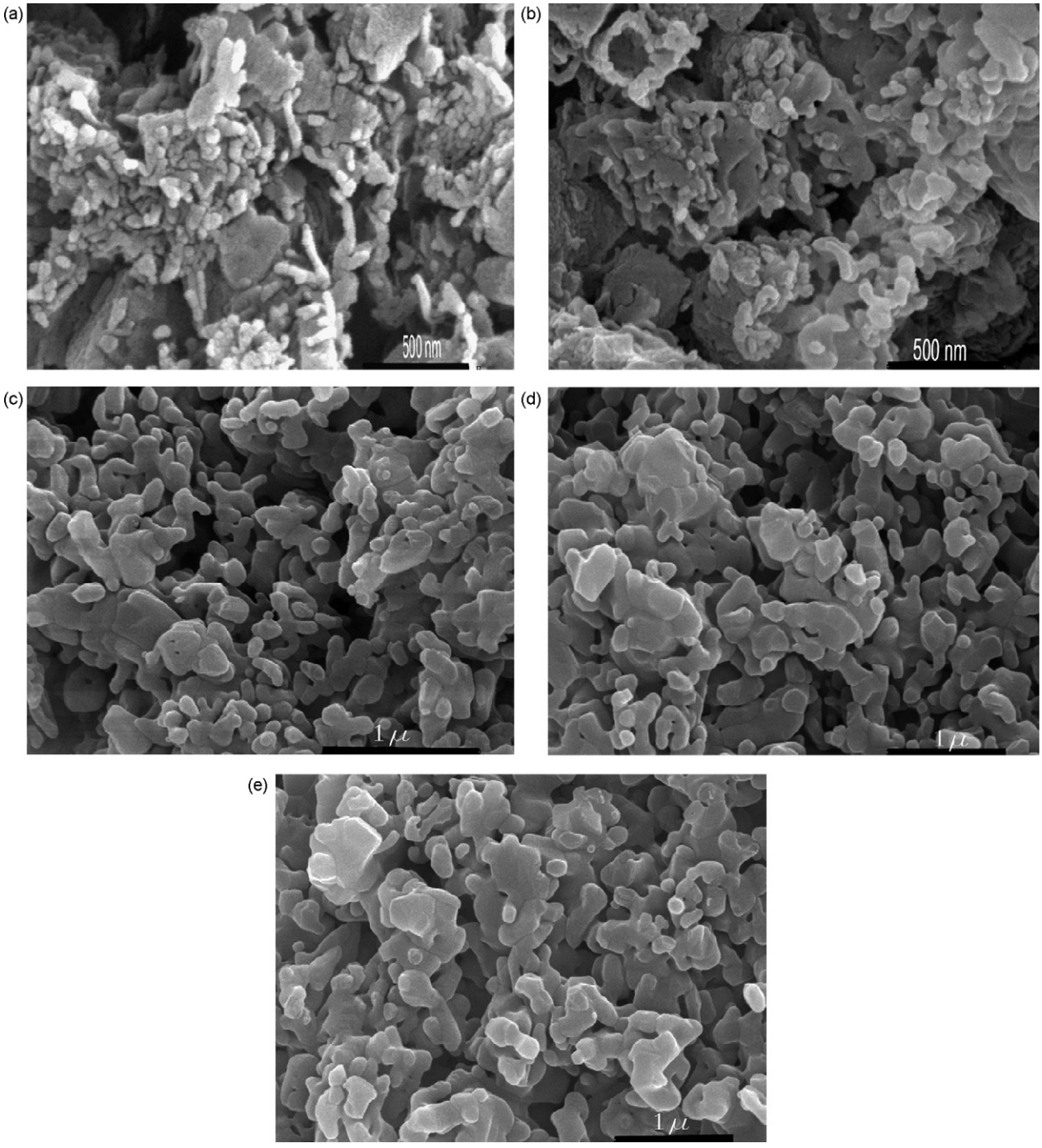

Fig. 7. (a) SEM of sample sintered at 1000 °C with 10 MPa applied pressure. (b) SEM of sample sintered at 1050 °C with 10 MPa applied pressure. (c) SEM of sample sintered at 1100 °C with 10 MPa applied pressure. (d) SEM of sample sintered at 1150 °C with 10 MPa applied pressure. (e) SEM of sample sintered at 1200 °C with 10 MPa applied pressure.

3.4. Microstructure evolution

The microstructure evolution with sintering temperature and pressure are shown in Figs. 7 and 8, respectively. At 1000 °C with 10 MPa, and 1050 °C with 10 and 20 MPa pressure, the microstructure predominantly consisted of extremely fine grains corresponding to those of transition alumina phases; fine pores were located between these grains forming a continuous network. Temperatures beyond 1050 °C led to gradual evolution of α-alumina phase with concomitant increase in grain size due to accelerated grain growth of the α-alumina phase; pores were rearranged into broader channels still maintaining the continuous network in the matrix.

The change in grain shape and morphology was also distinctly evident from the micrographs. The microstructure was irregular up to 1050 °C due to retention of the morphology of the starting $Al(OH)_3$ particles. Beyond 1050 °C it gradually became regular with more and more θ to α phase

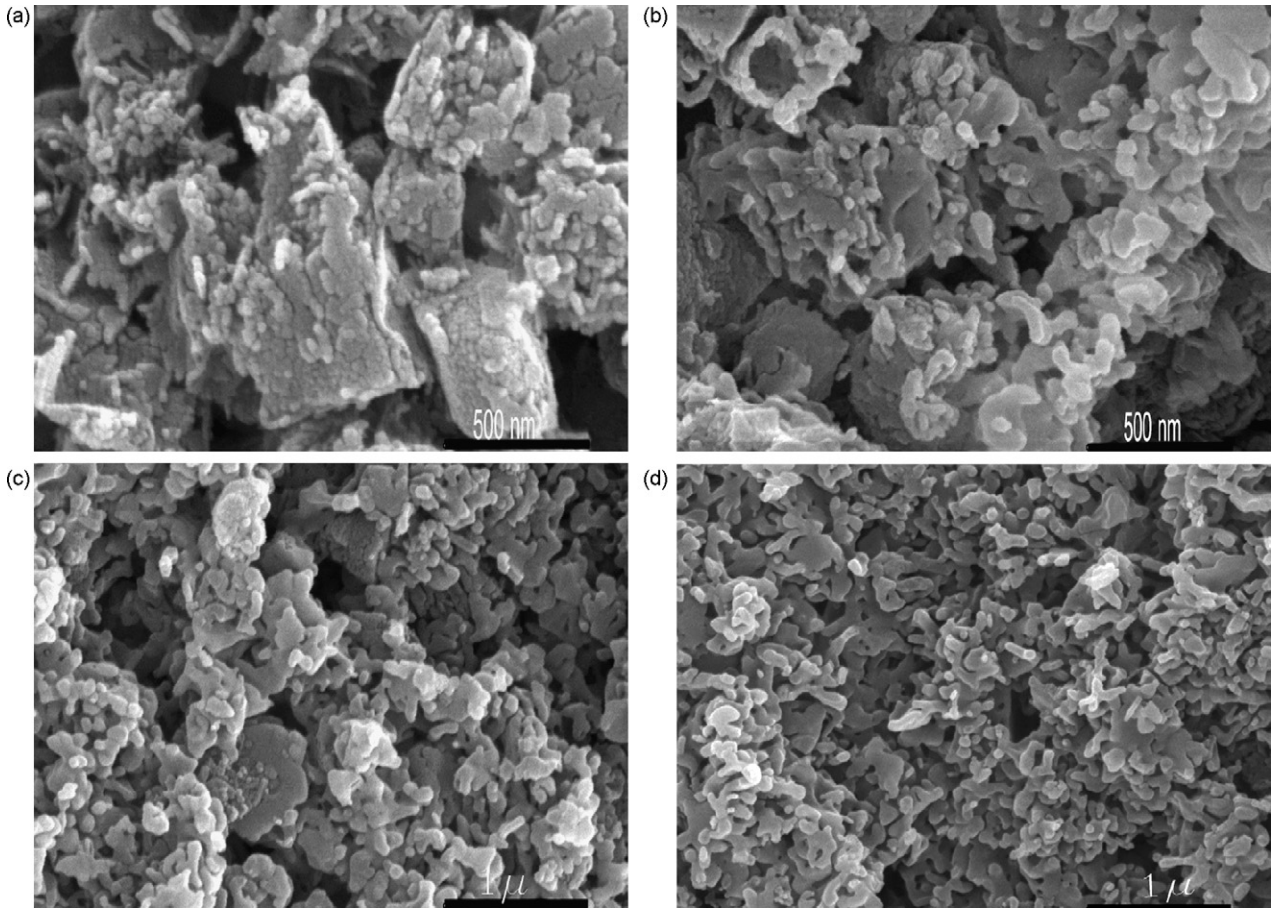

Fig. 8. (a) SEM of sample sintered at 1050 °C with 10 MPa applied pressure. (b) SEM of sample sintered at 1050 °C with 20 MPa applied pressure. (c) SEM of sample sintered at 1050 °C with 30 MPa applied pressure. (d) SEM of sample sintered at 1050 °C with 50 MPa applied pressure.

transformation. At 1100 °C the grain shape and morphology were markedly different; the grains were distinct and the microstructure was 'open' and predominantly fine grained with a few bigger grains also visible. At 1150 °C extensive necking was observed and the microstructure was less porous. At 1200 °C there was some grain growth and the microstructure became more 'closed' though the porous structure was still retained.

3.5. Surface area and bending strength

Surface area of the porous sintered samples increased with decreasing sintering temperature due to retention of fine pores and fine grained transition alumina phases at lower temperatures. Surface area as high as 80 ± 5 and $58 \pm 5\ m^2/g$ were obtained at sintering temperatures of 1000 and 1050 °C, respectively. With gradual transformation of the transition phases to α-alumina with temperature and pressure, the surface area decreased and the bending strength increased due to decrease in porosity. As θ-alumina has fine grain size and a large surface area, retaining a high percentage of θ-alumina is desirable to get a porous alumina body; however in such cases the strength of the specimen decreases due to inherent poor strength of the θ-alumina phase. Saito et al.[19] have added silica to $Al(OH)_3$ to retain the θ-alumina phase up to higher temperatures by reducing the surface contact between θ- and α-alumina particles.

The bending strength of samples sintered at different temperature and pressure along with the corresponding surface area, porosity and average grain size are given in Table 1. As surface diffusion predominates in the sintering of nanopowders, grain boundary strengthening occurs due to necking at relatively lower temperatures. The exothermic θ- to α-alumina phase transformation accelerates necking which yields a porous alumina structure with fracture strength as high as 400 MPa at 1050 °C and 50 MPa pressures. It also results in stronger grain bonding, as the bonding area was larger, due to the finer alumina grains produced by decomposition of $Al(OH)_3$. Considering the microstructures from Figs. 7 and 8 it may be interpreted that bending strength increases with increase in neck size. Amount of necking increased with temperature and pressure leading to higher strength values. The bending strength obtained in this work is higher compared to alumina and Al_2O_3-SiC nanocomposites[12] at identical porosity as shown in Fig. 9 although this work does not include any hard phase dopants, additives or inclusions to enhance strength. Another interesting point in this comparison is that the strength increases rapidly with increasing sintering temperature without compromising much in porosity unlike in

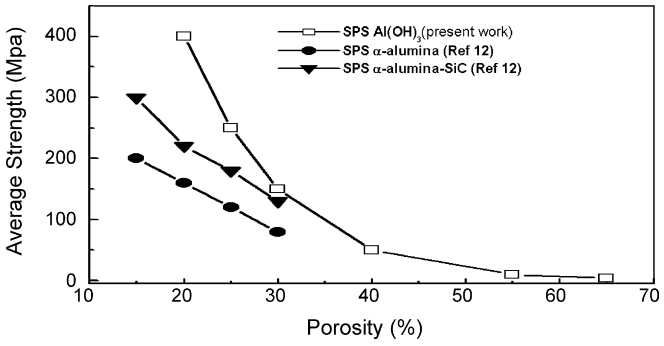

Fig. 9. Effect of porosity on bending strength.

the case of SPS sintered α-Al_2O_3 with SiC additive[12] where the porosity drastically decreases with increasing strength. However, strength values reported by Jayaseelan et al.[13] were higher as they used MgO and TiO_2 as additives and sintered at 1200 °C as compared to 1050 °C in this work.

3.6. Advantage of spark plasma sintering

SPS is an attractive technique for synthesizing porous ceramic components because of grain boundary strengthening as well as phase transformation occurring at relatively lower temperatures due to simultaneous application of current and pressure leading to rapid heating rates enabling shorter sintering schedules. The low sintering temperature and short holding time in SPS helped retain the fine pores and narrow pore size distribution in the alumina matrix. In SPS, preferential necking takes place between powder particles due to local resistive heating.[20] Besides, it is speculated that electric discharge occurs between particles and probably some plasma is also formed[20] all of which lead to local temperature increments at points of contact between particles. Hence, with increase in temperature an increase in neck size is expected. Presumably, extensive necking was evident from the microstructures, which led to enhanced strength even at lower sintering temperatures compared to conventional sintering[6] and hot pressing.[10] Also, the abundance of fine alumina grains led to strong grain bonding on passing pulsed dc current in SPS, giving sintered specimens with sufficiently high strength.

4. Conclusion

1. Alumina based porous ceramics was fabricated using SPS technique with $Al(OH)_3$ as the starting powder. No additives, dopants or inclusions were added during the process. $Al(OH)_3$ was prepared initially by hydrolysis of nano-aluminum powder.
2. The decomposition of $Al(OH)_3$ during sintering produced a series of transitional alumina phases with increase in temperature and pressure, and finally a highly porous nanocrystalline stable α-alumina phase was obtained.
3. SPS parameters were optimized at 1050 °C/30 MPa to obtain alumina samples having a continuous network of nanopores with bending strength high enough to be used as devices for medical applications.
4. Pore sizes and size distributions as estimated by mercury porosimetry and BET analysis showed that the pores were unimodal in distribution at all temperatures and pressures. The pore size distribution became wider and the distribution peak gradually shifted towards larger size with increased sintering temperature and pressure. This is probably due to decomposition of $Al(OH)_3$ followed by a volume shrinkage during θ- to α-alumina phase transformation.
5. High surface area was due to the retention of fine pores and fine grained transition alumina phases at lower temperatures; surface area decreased with increasing temperature as α-alumina phase formation took place.
6. Bending strength increased with sintering temperature and pressure due to extensive necking among grains and the predominance of fine α-alumina grains in the microstructure leading to stronger grain bonding on passing pulsed dc current during SPS.
7. Grain size increased with temperature due to accelerated grain growth of the α-alumina phase; pores were rearranged into broader channels still maintaining the continuous network in the matrix. The ‘open’ microstructure at lower temperatures became a more ‘closed’ one with increasing temperature and pressure.

Acknowledgement

The authors are grateful to Dr. G. Sundararajan, Director ARCI, for permitting to carry out this work. The authors also thank Dr. G.V.N. Rao, Dr. Roy Johnson, Dr. U.S. Hareesh and Mr. L. Venkatesh for characterization of the samples. Dr. P.K. Das from CGCRI, Kolkata is gratefully acknowledged for carrying out the bending tests of the samples.

References

1. Deng, Z. Y., Fukasawa, T., Ando, M., Zhang, G. J. and Ohji, T., High-surface-area alumina ceramics fabricated by the decomposition of $Al(OH)_3$. *J. Am. Ceram. Soc.*, 2001, **84**, 485–491.
2. Falamaki, C., Afarani, M. S. and Aghaie, A., Initial sintering stage pore growth mechanism applied to the manufacture of ceramic membrane support. *J. Eur. Ceram. Soc.*, 2004, **24**, 2285–2292.
3. McArdle, J. L. and Messing, G. L., Transformation, microstructure development, and densification in α-Fe_2O_3 seeded boehmite derived alumina. *J. Am. Ceram. Soc.*, 1993, **76**, 214–222.
4. Wu, S. J. and De Jonghe, L. C., Sintering of nanophase γ-Al_2O_3 powder. *J. Am. Ceram. Soc.*, 1996, **79**, 2207–2211.
5. Yen, T. S. and Sacks, M. D., Low-temperature sintering of aluminum oxide. *J. Am. Ceram. Soc.*, 1988, **71**, 841–844.
6. Deng, Z. Y., Fukasawa, T., Ando, M., Zhang, G. J. and Ohji, T., Microstructure and mechanical properties of porous alumina ceramics by the decomposition of aluminum hydroxide. *J. Am. Ceram. Soc.*, 2001, **84**, 2638–2644.
7. Pierre, A. C., Porous sol–gel ceramics. *Ceram. Int.*, 1997, **23**, 229–238.
8. Lyckfeldt, O. and Ferreira, J. M. F., Processing of porous ceramics by starch consolidation. *J. Eur. Ceram. Soc.*, 1995, **18**, 131–140.
9. Hardy, D. and Green, D. J., Mechanical properties of a partially sintered alumina. *J. Eur. Ceram. Soc.*, 1995, **15**, 769–775.
10. Ostrowski, T. and Rödel, J., Evolution of mechanical properties of porous alumina during free sintering and hot pressing. *J. Am. Ceram. Soc.*, 1999, **82**, 3080–3086.

11. Claussen, N., Wu, S. X. and Holz, D., Reaction bonding of aluminum oxide (RBAO) composites: processing, reaction mechanisms and properties. *J. Eur. Ceram. Soc.*, 1994, **14**, 97–109.
12. Oh, S. T., Tajima, K. I., Ando, M. and Ohji, T., Strengthening of porous alumina by pulsed electric current sintering and nanocomposite processing. *J. Am. Ceram. Soc.*, 2000, **83**, 1314–1316.
13. Jayaseelan, D. D., Kondo, N., Brito, M. E. and Ohji, T., High-strength porous alumina ceramics by the pulse electric current technique. *J. Am. Ceram. Soc.*, 2002, **85**, 267–269.
14. Jigatch, A. N., Leipunskii, I. O., Kuskov, M. L., Stoenko, N. I. and Storozhev, V. B., An apparatus for the production and study of metal nanoparticles. *Instrum. Exp. Tech.*, 2000, **43**, 839–845.
15. Standard Test Method for Water Absorption, Bulk Density, Apparent Porosity, and Apparent Specific Gravity of Fired Whiteware Products, ASTM C, 373-88, 2006.
16. Standard Test Method for Biaxial Flexure Strength (Modulus of Rupture) of Ceramic Substrates, ASTM F, 394-78, 1978, pp. 434–440.
17. Kao, H. C. and Wei, W. C., Kinetics and microstructural evolution of heterogeneous transformation of θ-alumina to α-alumina. *J. Am. Ceram. Soc.*, 2000, **83**, 362–368.
18. Shi, J. L., Solid state sintering of ceramics: pore microstructure models, densification equations and applications. *J. Mater. Sci.*, 1999, **34**, 3801–3812.
19. Saito, Y., Takei, T., Hayashi, S. and Okada, K., Effects of amorphous and crystalline silica additives on θ-alumina to α-alumina phase transition. *J. Am. Ceram. Soc.*, 1998, **81**, 2197–2200.
20. Gao, L., Shen, Z., Miyamoto, H. and Nygren, M., Superfast densification of oxide/oxide ceramic composite. *J. Am. Ceram. Soc.*, 1999, **82**, 1061–1063.